JOURNAL OF CATALYSIS **176,** 155–172 (1998)
ARTICLE NO. CA982009

Bifunctional Condensation Reactions of Alcohols on Basic Oxides Modified by Copper and Potassium

Marcelo J. L. Gines and Enrique Iglesia[1]

Department of Chemical Engineering, University of California at Berkeley, Berkeley, California 94710

Received September 9, 1997; revised January 12, 1998; accepted January 20, 1998

Alcohol dehydrogenation and condensation reactions are involved in chain growth pathways on $Cu/MgCeO_x$ promoted with potassium. These pathways lead to the formation of isobutanol with high selectivity via reactions of higher alcohols with methanol-derived C_1 species in reaction steps also relevant to higher alcohol synthesis from CO/H_2 mixtures at higher pressures on $K-Cu/MgCeO_x$ catalysts. Ethanol reactions on $K-Cu_yMg_5CeO_x$ show that both Cu and basic sites participate in alcohol dehydrogenation and aldol condensation steps leading to n-butyraldehyde and acetone. Chain growth occurs by condensation reactions involving a metal-base bifunctional aldol-type coupling of alcohols. Reactions of $^{12}C_2H_5OH-^{13}C_2H_4O$ mixtures show that direct condensation reactions of ethanol can occur without requiring the intermediate formation of gas phase acetaldehyde. Reactions of C_2H_5OH/D_2 mixtures show that Cu sites increase the rate of aldol condensation by introducing recombinative desorption sites that remove hydrogen atoms formed in C–H activation steps leading to the unsaturated aldol-type species required for chain growth. Reactions of acetaldehyde and ^{13}C-labeled methanol lead predominantly to 1-^{13}C-propionaldehyde and 2-^{13}C-isobutyraldehyde, both of which lead to isobutanol during CO/H_2 reactions. Mixtures of propionaldehyde and ^{13}C-labeled methanol lead to singly-labeled isobutyraldehyde. Chain growth to C_{2+} alcohols occurs via addition of a methanol-derived C_1 species to adsorbed oxygen-containing intermediates. The gradual appearance of ^{13}C in the unlabeled reactant within these mixtures shows that aldol coupling reactions are reversible. Reverse aldol condensation reactions after intramolecular hydride transfer lead to the formation of acetone from ethanol. Isobutyraldehyde is a preferred end-product of aldol-type chain growth reactions of alcohols because it lacks the two α-hydrogens required for subsequent chain growth.

1. INTRODUCTION

Isobutanol is a useful intermediate in the synthesis of methyl-tert-butyl-ether after its dehydration to isobutene and further etherification with methanol. Currently available catalysts for the synthesis of isobutanol from CO/H_2 mixtures with high productivity (>100 g/kg cat-h) require high temperatures (750–800 K) and pressures (10–30 MPa) (1–5). These catalysts produce isobutanol with relatively low rates and selectivity at lower temperatures and pressures. Alkali-modified methanol synthesis catalysts produce higher alcohols from CO/H_2 mixtures at lower temperature (583 K) and pressures (7.6 MPa) (6–9). These catalysts produce a mixture of linear and branched alcohols and maximum isobutanol productivities are 48.6 g/kg cat-h (8). Recently, $K-Cu-Mg-CeO_x$ materials have been shown to catalyze higher alcohol synthesis at low temperatures and pressures (10–13). These bifunctional catalysts consist of Cu crystallites supported on high surface area basic oxides based on K-modified MgO.

Isobutanol synthesis requires the initial formation of methanol and higher linear alcohols and their subsequent chain growth leading to 2-methyl-branched alcohols with high selectivity (3 and references therein). Cu metal sites catalyze methanol synthesis and hydrogenation–dehydrogenation reactions of aldehydes and alcohols (14, 15). Solids based on MgO catalyze condensation reactions of alcohols and aldehydes with high selectivity (16, 17). Also, MgO is an active and selective catalyst for Guerbet condensation reactions of primary C_2-C_5 alcohols with methanol (18, 19).

The mechanism of methanol synthesis from $CO_2/CO/H_2$ mixtures has been extensively studied (20–25). Methanol synthesis involves the formation of a formate species via the reaction of CO_2 with H-adatoms, followed by a rate-determining hydrogenolysis step (22–25). Bowker *et al.* (22) reported that the mechanism by which methanol is made on $Cu/ZnO/Al_2O_3$ from $CO_2/H_2/He$ and $CO_2/CO/H_2$ feeds is by the co-adsorption of hydrogen and carbon dioxide on the copper component of the catalyst, forming surface formate species, which undergo hydrogenation/hydrogenolysis reactions to yield methanol. Robbins *et al.* (24) showed that from $CO/CO_2/H_2$ feeds the rate of methanol formation on Cu/SiO_2 catalysts is proportional to Cu surface area, suggesting that metallic Cu is the active catalytic component. In CO_2-free feeds, the synthesis rate, however, is not proportional to the Cu surface area, indicating that other types of catalytic sites are involved. They suggested that surface hydroxyls might be

[1] Corresponding author. E-mail address: iglesia@cchem.berkeley.edu.

0021-9517/98 $25.00

required for the initial conversion of CO to adsorbed formate. Using diffuse reflectance infrared Fourier transform (DRIFTS) and temperature-programmed reaction spectroscopies (TPRS), Neophytides *et al*. (25) found that methanol synthesis on a $Cu/ZnO/Al_2O_3$ commercial catalyst occurs via the rate-limiting hydrogenation of copper formate. Recently, it has been proposed that methanol synthesis from carbon oxide/hydrogen mixtures involves the generation of a formate species on the copper surface, the formate species then migrates onto ZnO, and is subsequently hydrogenated to methanol (26). Temperature-programmed infrared (TPIR) spectroscopy of copper formate/ZnO showed the migration of surface formate species from copper to ZnO at temperatures below 430 K and the beginning of copper formate decomposition above 430 K (26).

The formation of C_{2+} linear alcohols during CO hydrogenation remains the least understood step and the rate of formation of ethanol appears to limit the overall rate of chain growth (4, 10). Several mechanisms have been proposed for the formation of the initial C–C bond:

(a) C–C bond formation by CO insertion into metal–carbon bonds in adsorbed formaldehyde species, observed on ZnO and ThO_2 catalysts (27);

(b) Coupling of two C_1 aldehydic intermediates on carbides (CaC_2, Na_2C_2, CeC_2, and LaC_2) (28);

(c) Methanol and ethanol formation from a common intermediate on $CuO/ZnO/Al_2O_3$ (29);

(d) Direct carbonylation of surface C_1 species (CH_3OH, H_2CO, and CH_3O^-) on $Cu/ZnO/Al_2O_3$ and Cs–Cu/ZnO catalysts (6, 30).

Our recent experiments using $^{13}CO/CH_3OH/H_2$ mixtures have shown that ethanol is formed directly from CO at short residence time on $K–Cu_{0.5}Mg_5CeO_x$ catalysts (31), but via methanol coupling reactions on $Cs–Cu/ZnO/Al_2O_3$ catalysts (6, 32).

After initial C–C bond formation steps, higher alcohol mixtures form via aldol condensation reactions of surface-bound aldehydic species (10). Aldol-type condensation reactions of alcohols in the liquid phase proceed via the following reaction steps (Scheme 1): alcohol dehydrogenation to form aldehydes (or ketones), α-hydrogen abstraction to form enolate species, nucleophilic addition of enolate to carbonyl species followed by dehydration to form α,β-unsaturated aldehyde (or ketone), and hydrogenation of the C=C and C=O bonds to form the corresponding alcohol (33).

On $CuO/ZnO/Al_2O_3$, linear 1-alcohols containing n carbons condense mainly to esters with 2n carbon atoms, ketones with 2n-1 carbons, and ketones with 2n atoms (Scheme 2) (34). On Cu/ZnO, the aldol-condensation reactions occur via the normal mechanism, but on Cs–Cu/ZnO the oxygen associated with the C_1 carbon source is retained

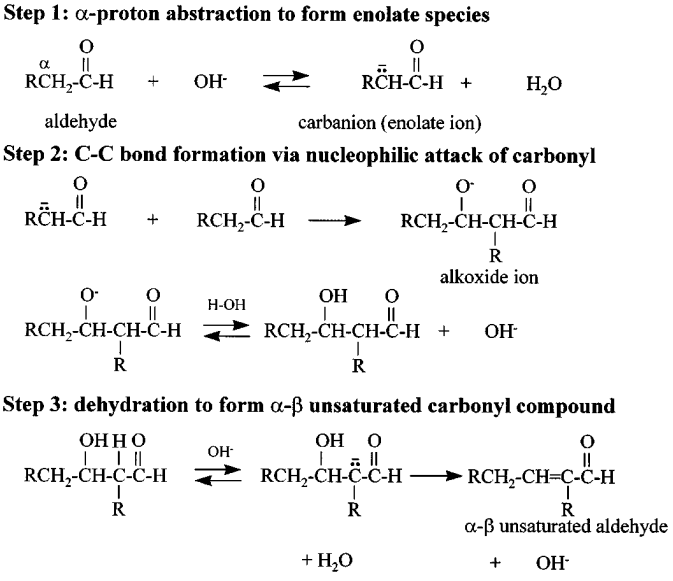

SCHEME 1. Homogenous aldol condensation of aldehydes (33).

in the C_2 to C_3 step (Scheme 3) (7, 8). The retention of oxygen associated with the C_1 intermediate is believed to be caused by the strong bonding of the alkyl oxygen in the di-oxygenated $RCH(H_2CO^-)CHO$ intermediate anion to Cs^+ cations, which prevents hydrogenation of the H_2CO^- group, while allowing complete hydrogenation of the free –CHO group to $-CH_3$ (7).

Here, we report kinetic and isotopic tracer studies of alcohol dehydrogenation and condensation reactions, with emphasis on chain growth pathways on $Cu/MgCeO_x$ solids promoted with potassium. Our results show that direct condensation reactions of ethanol occurs without the intermediate formation of gas phase acetaldehyde, that Cu sites increase the rate of aldol condensation by introducing recombinative desorption sites that disposal hydrogen

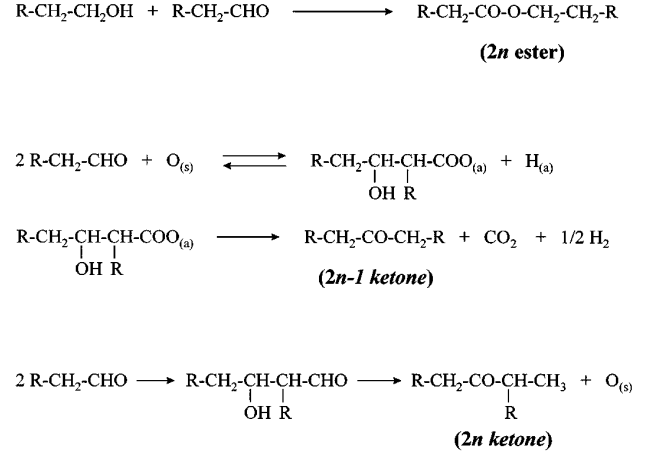

SCHEME 2. Pathways to higher oxygenates (34).

normal aldol condensation:

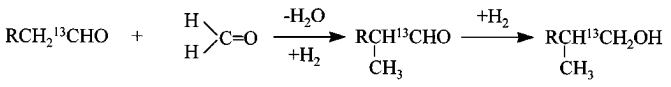

aldol coupling with oxygen retention reversal:

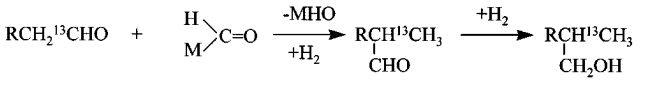

R may be a hydrogen atom or methyl group; M=catalyst or H in surface bonded formaldehyde

SCHEME 3. Normal and reversal aldol condensation according to Nunan *et al.* (7).

atoms formed in C–H activation steps, and that chain growth to C_{2+} alcohols occurs via addition of a C_1 species to adsorbed oxygenates. Based on these findings, we propose that chain growth occurs by condensation reactions involving a metal-base bifunctional mechanism.

2. EXPERIMENTAL METHODS

2.1. Catalyst Synthesis

Cu–Mg–CeO_x samples were prepared by coprecipitation of mixed metal nitrate solutions with an aqueous solution of KOH (2*M*) and K_2CO_3 (1*M*) at 338 K and a constant pH of 9 in a well-stirred thermostated container (13). The solids formed were filtered, washed thoroughly with 300–500 cm^3 of deionized water at 333 K, and dried at 353 K overnight. Dried samples were treated in flowing air at 723 K for 4 h in order to form the corresponding mixed metal oxides. Residual potassium in all dry samples was less than 0.1 wt% before alkali impregnation. K was introduced by incipient wetness of the oxidized samples using 0.25*M* K_2CO_3 aqueous solutions (K_2CO_3: Fisher Scientific, A.C.S. Certified). The properties of the synthesized samples are listed in Table 1.

2.2. Catalyst Characterization

Powder X-ray diffraction (XRD) spectra were obtained using a D5000 Siemens Diffractometer and monochromatic Cu-K_α radiation. Total surface areas were determined using the single point BET method by measuring N_2 physisorption at 77 K using a continuous flow Quantasorb Surface Area Analyzer (Quantachrome Corp.). Bulk catalyst compositions were measured by atomic absorption spectroscopy (AAS).

Cu surface areas in reduced samples were measured by titrating Cu surface atoms with N_2O (Matheson, ultra high purity) at 363 K. N_2O was introduced as pulses (1.60 μmol N_2O/pulse) into a He stream. The number of chemisorbed oxygen atoms was obtained from the amount of N_2O consumed or N_2 produced. A saturation coverage of 0.5 : 1 O : Cu_s was used to estimate Cu surface area and dispersion (35–37). Cu dispersion is defined as the ratio of surface Cu (Cu_s) to the total number of Cu atoms in the catalyst.

The density of basic sites was determined using a $^{13}CO_2/^{12}CO_2$ exchange method at 573 K. This method provides a direct measure of the number of sites that can *reversibly* interact with CO_2 at typical reaction temperatures. Detailed descriptions and experimental procedures and methods are reported elsewhere (13, 38).

2.3. Catalytic Evaluation and Mechanistic Studies

2.3.1. Ethanol reactions. Ethanol reactions were carried out in a gradientless recirculating batch reactor at 573 K and 101.3 kPa. Catalyst samples (18.0 mg) were first reduced in H_2 (10% H_2/He, 175 cm^3/min, 5 K/min) at 623 K for 0.5 h. The temperature was lowered to 573 K and ethanol was introduced along with a small amount of methane, which was used as an unreactive internal standard in order to ensure accurate mass balances ($C_2H_5OH/CH_4/He$ = 4.0/2.7/94.6 kPa; C_2H_5OH, Fisher Scientific, A.C.S. certified; CH_4, Matheson, ultra high purity). H_2 was purified by passing through a catalytic purifier (Matheson, Model 64-1008). Traces of water were removed from H_2 and helium using molecular sieves (Matheson, Model 452 : 4A). CH_4 was used without further purification. The reactant mixture was circulated continuously through the catalyst bed and reaction products were sampled by syringe extraction after various contact times. Reactants and products were analyzed using a dual detector gas chromatograph (Hewlett-Packard, Model 5890 II Plus; TCD/FID detectors). One sample was injected into a 5% phenyl-methyl-silicone capillary column (HP-1, 50 m, 0.32 mm diameter, 1.05 μm film thickness) and the other into a packed column (Porapak Q,

TABLE 1

Composition, Surface Area, and Basic Site Density of Mixed Metal Oxides

Sample	Cu content (wt%)	K[a] content (wt%)	BET surface area (m^2/g)	Cu[b] dispersion	Exchangeable CO_2 at 573 K (10^{-6} mol/m^2)
Mg_5CeO_x	0	0.01	188	—	0.95
Mg_5CeO_x	0	0.8	155	—	1.7
$Cu_{0.5}Mg_5CeO_x$	7.7	0.1	167	0.23	1.2
$Cu_{0.5}Mg_5CeO_x$	7.7	1.0	147	0.14	2.3
$Cu_{7.5}Mg_5CeO_x$	49	1.2	92	0.047	3.3

[a] Bulk composition measured by atomic absorption.

[b] Dispersion calculated from the ratio of the number of surface Cu (determined by N_2O decompositon at 363 K (35, 36, 37)) to the total number of Cu atoms in the catalyst.

1.8 m length, 0.32 cm diameter). A thermal conductivity detector (TCD) was used to measure the concentration of CO, CO_2, and C_2H_5OH in the effluent from the packed column. A flame ionization detector (FID) was used to measure the concentrations of all organic compounds eluting from the capillary column. Products were also analyzed by mass spectrometry after capillary chromatography in order to confirm the chemical identity and to determine the isotopic compositions of reactants and products (Hewlett-Packard, Model 5890 II Plus GC; Hewlett-Packard, Model 5972 Mass Selective Detector).

Reaction rates are reported as turnover rates, defined as the moles of reactant converted to products per unit time and per g-atom surface site. The local slope of turnover-time plots gives the turnover rate for the formation of each product. Turnovers (for reactants) or site-yields (for each product) are defined as the moles of reactant converted to a given product per gram-atom surface sites in the reactor. When divided by the fractional Cu dispersion, this becomes a site-time yield for each product, at least for reactions with rate-determining elementary steps requiring Cu surface atoms. Also, the total surface area, the $MgCeO_x$ surface area (estimated from the difference between the total surface area and the copper surface area) and the number of basic sites from CO_2 exchange were used in order to normalize reaction rates. The choice among these values depends on which sites or surfaces are required for the rate-determining elementary step in the overall catalytic sequence.

2.3.2. Reactions of acetaldehyde. Condensation and hydrogenation reactions of acetaldehyde were examined on 0.8 wt% K–Mg_5CeO_x, 1.0 wt% K–$Cu_{0.5}Mg_5CeO_x$, and 1.2 wt% K–$Cu_{7.5}Mg_5CeO_x$. The catalyst (33.0 mg) was first reduced in H_2 (10% H_2/He) at 623 K for 0.5 h. The reaction was carried out at 573 K. The reactant mixture was: $C_2H_4O/CH_4/He = 6.6/2.7/92.0$ kPa (C_2H_4O, Fisher Scientific, Reagent Grade; CH_4, Matheson, ultra high purity). Reaction products were analyzed by the procedures described in the previous section.

2.3.3. Reactions of $C_2H_5OH/^{13}C_2H_4O$ mixtures. Competitive reactions between $^{12}C_2H_5OH$ and $^{13}C_2H_4O$ were examined on 0.8 wt% K–Mg_5CeO_x, 1.0 wt% K–$Cu_{0.5}Mg_5CeO_x$, and 1.2 wt% K–$Cu_{7.5}Mg_5CeO_x$ catalysts in order to probe direct pathways from ethanol to condensation products and the role of acetaldehyde intermediates. The catalyst (22.0 mg) was reduced in 10% H_2 (balance He) at 623 K for 0.5 h. Reactions were conducted at 523 K and 101.3 kPa in the recirculating reactor unit. The reactant mixture was introduced along with a small amount of methane (reaction mixture: $^{13}C_2H_4O/^{12}C_2H_5OH/H_2/CH_4/He = 2.9/1.1/2.9/2.4/92.0$ kPa; $^{13}C_2H_4O$: Isotec Inc., ^{13}C: 99%; C_2H_5OH: Fisher Scientific, A.S.C. Certified; CH_4: Matheson, ultra high purity). ^{13}C content and isotopic distributions in reactants and products were analyzed by mass spectrometry using a matrix deconvolution method that accounts for the natural ^{13}C abundance and mass fragmentation patterns of each molecule (39).

2.3.4. Reactions of C_2H_5OH/D_2 mixtures. Reactions of C_2H_5OH/D_2 mixtures were carried out in a gradientless recirculating batch reactor in order to probe the rate of recombinative hydrogen desorption during ethanol coupling reactions. Catalyst samples (20.0 mg) were treated in H_2 (10% H_2/He, 175 cm^3/min, 5 K/min) at 623 K for 0.5 h. The temperature was then decreased to 573 K and the reactant mixture was introduced along with a small amount of methane (reaction mixture: $C_2H_5OH/CH_4/D_2/He = 3.6/2.4/27.0/68.3$ kPa; C_2H_5OH, Fisher Scientific, A.C.S. certified; CH_4, Matheson, ultra high purity; D_2, C.P. Matheson). Products were sampled by syringe extraction from the recirculating stream at different contact times and analyzed as described in Section 2.3.1. The deuterium content in reactants and products was measured by mass spectrometry using previously reported deconvolution methods (39).

2.3.5. Cross-coupling reactions of $^{13}CH_3OH/C_2H_4O$ and $^{13}CH_3OH/C_3H_6O$ mixtures. Cross-coupling reactions of $^{13}CH_3OH$ (^{13}C, 99%,^{18}O, <1%, Icon Services Inc.) with acetaldehyde (Fisher Scientific, Reagent Grade) and propionaldehyde (Aldrich, 97%) were carried out using the following reactant mixture: $^{12}C_2H_4O(^{12}C_3H_6O)/^{13}CH_3OH/CH_4/He = 7.3/4.0(4.0)/2.7/87.3$ kPa. $^{13}CH_3OH$ was purified by several freeze-pump-thaw cycles before catalytic experiments. Reactions were conducted at 573 K and 101.3 kPa in a recirculating reactor unit. Mass spectrometry analysis after chromatographic separation was used to confirm the identity of each reaction product and to determine ^{13}C content, position, and distributions in reactants and products.

3. RESULTS AND DISCUSSION

3.1. Structural and Textural Properties of K–Cu–Mg–CeO_x Catalysts

The composition, surface area, Cu dispersion, and density of basic sites for mixed metal oxides are shown in Table 1. Copper dispersion decreased with increasing K loading (Table 1), because the presence of alkali decreases Mg_5CeO_x surface area, blocks surface Cu atoms, and inhibits Cu^{2+} reduction to Cu metal (13). The addition of K also decreased the total surface area of $Cu_{0.5}Mg_5CeO_x$ samples (Table 1). The copper dispersion in $Cu_{0.5}Mg_5CeO_x$ is 0.23 (Table 1); this value is among the highest reported in the literature for Cu-based methanol and higher alcohol synthesis catalysts. The density of basic sites obtained by isotopic CO_2 exchange methods on MgO at 573 K is 0.38×10^{-6} mol/m^2; this is lower than the value of 18.3×10^{-6} mol/m^2 reported for the surface density of oxygen atoms in MgO (40). This is not unexpected because the $^{13}CO_2/^{12}CO_2$ isotopic switch method detects only those

basic sites that interact reversibly with CO_2 at 573 K in typical catalytic turnover times (13, 38). The basic site density increased from 1.2 to 2.3×10^{-6} mol/m^2 with increasing K loading from 0.1 to 1.0 wt%. Small amounts of CeO_x in MgO (Mg/Ce = 5 at.) increased the density of basic sites (Table 1).

$Mg(OH)_2$ and $Ce(OH)_4/CeO_2$ phases were identified by X-ray diffraction on dried precipitate samples. The poor sample crystallinity and the coincidence of diffraction lines for Ce oxide and hydroxide phases make it difficult to determine conclusively the form of Ce in dried samples. No layered hydrotalcite-type structures were detected by X-ray diffraction. Samples calcined at 723 K exhibited separate MgO and CeO_2 phases. Diffraction lines provided no evidence for $MgCeO_x$ mixed oxides. CuO crystallites were not detected, suggesting that the Cu component is well dispersed, either as small crystallites or as a solid solution within the CeO_2 lattice. Mixed Cu/Ce oxide solid solutions can form during co-precipitation and remain after high temperature oxidative treatments (41, 42).

3.2. *Ethanol Reactions*

Ethanol dehydrogenation and coupling reactions were studied in order to probe reaction pathways involved in branched and linear higher alcohol syntheses from methanol, ethanol, and propanol intermediates formed initially during CO hydrogenation reactions at high pressures. These studies also address the roles of Cu, K, and Mg–Ce oxides in ethanol coupling reactions. The experiments were carried out on Mg_5CeO_x, 0.8 wt% K–Mg_5CeO_x, $Cu_{0.5}Mg_5CeO_x$, 1.0 wt% K–$Cu_{0.5}Mg_5CeO_x$, and 1.2 wt% K–$Cu_{7.5}Mg_5CeO_x$ at atmospheric pressure.

Acetaldehyde was the predominant product of reactions of pure ethanol on 1.0 wt% K–$Cu_{0.5}Mg_5CeO_x$ (Fig. 1). Dehydrogenation reactions occur much faster than chain growth; the latter reaction leads to the formation of acetone,

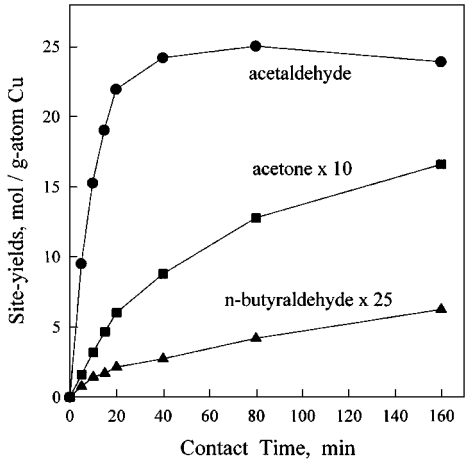

FIG. 1. Site yields as a function of contact time on 1.0 wt% K–$Cu_{0.5}Mg_5CeO_x$ in ethanol reactions (573 K, 101.3 kPa total pressure, 4.0 kPa ethanol, balance He).

n-butyraldehyde, and other oxygenates. Acetaldehyde reaches a maximum concentration at intermediate contact times during ethanol reactions and then decreases gradually. The acetaldehyde concentration at this point corresponds to the acetaldehyde concentration calculated from the thermodynamic equilibrium of the chemical reaction:

$$C_2H_5OH \rightleftarrows C_2H_4O + H_2.$$

The small decrease in acetaldehyde concentration at long contact times could be caused by further reaction of acetaldehyde to secondary products and/or by the reversal of the ethanol-acetaldehyde equilibrium as ethanol is converted to chain growth products. Acetone and n-butyraldehyde were the predominant condensation products. The non-zero initial slopes on acetone and n-butyraldehyde curves (Fig. 1) are inconsistent with their formation only in sequential reactions of gas phase acetaldehyde intermediates such as

$$C_2H_5OH \rightleftarrows C_2H_4O \rightarrow \text{Condensation products.}$$

Therefore, condensation products are either formed directly by ethanol self-condensation or from acetaldehyde, but at reaction rates independent of acetaldehyde concentration. Methyl-ethyl ketone (by acetaldehyde self-condensation with intramolecular hydride shift before dehydration) (7, 8), 2-pentanone (by acetaldehyde-acetone condensation), 2-propanol (by hydrogenation of acetone), 1-butanol (by hydrogenation of n-butyraldehyde), and ethyl acetate (by ethanol-acetaldehyde) were also detected in much smaller concentrations than n-butyraldehyde and acetone among reaction products.

The formation of all detected products of ethanol reactions on K–Cu–Mg_5CeO_x catalysts can be described by the reaction pathways shown in Scheme 4. Acetaldehyde is formed via ethanol dehydrogenation (step I). Self-condensation of acetaldehyde (or surface acetaldehyde formed from dissociative adsorption of ethanol and sequential α-hydrogen abstraction) leads to the formation of n-butyraldehyde (steps II–IV) and methyl-ethyl ketone (steps II–V) (34). Enolate species can convert to the keto form via intramolecular H transfer (step VI); methyl-ethyl ketone can then be formed by dehydration-dehydrogenation reactions of this keto form (step VII). Acetone can form via two pathways: (i) by reaction of aldol intermediates with surface lattice oxygen to form the β-keto acid followed by decarboxylation (steps VIII–IX) and/or (ii) by reverse aldol reactions of the keto form of reaction intermediates (step X). Formaldehyde formed in the latter reaction decomposes rapidly to CO and H_2. Surface lattice oxygen consumed by reaction (IX) can be replenished by water and CO_2 formed in condensation reactions; 2-pentanone is formed by condensation of aldol-type intermediates formed in acetone-acetaldehyde reactions (steps XI–XII). Diethyl ether was only detected in trace

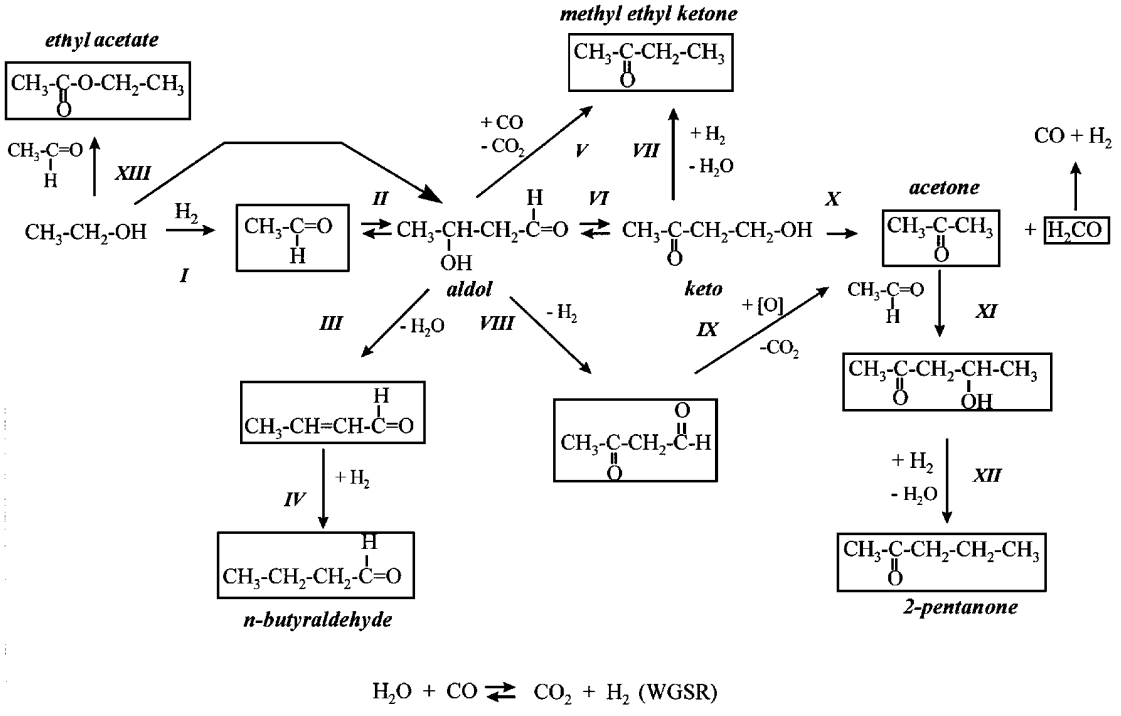

SCHEME 4. Reaction scheme for ethanol reactions on K–Cu–Mg_5CeO_x catalysts.

amounts on Mg_5CeO_x catalysts, and it is formed on CeO_x acid sites by dehydration of ethanol. Ethyl acetate can form by reactions of ethanol with acetaldehyde (step XIII) (34).

Ethanol reaction rates and the selectivities to acetaldehyde, n-butyraldehyde, and acetone were measured on K–Cu–$MgCeO_x$ catalysts with a range of Cu and K contents in order to examine the role of Cu and basic sites on dehydrogenation and condensation reactions. The results are shown in Table 2. Initial reaction rates were obtained from the slope of the site-yield plots at short contact times using the total surface area, the $MgCeO_x$ surface area (estimated from the difference between the total surface area and the copper surface area), the number of basic sites from CO_2 exchange, or the Cu metal surface area of each sample in order to normalize reaction rates.

Initial dehydrogenation rates were very low on both Mg_5CeO_x and 0.8 wt% K–Mg_5CeO_x catalysts and ethanol conversion reached a limiting value of about 9% after 0.33 h; this conversion value is much lower than the predicted equilibrium conversion (90%) at these reaction conditions. The decrease in ethanol conversion rates with increasing conversion may reflect (1) the formation of surface polymeric species from acetaldehyde and/or (2) an inhibition effect of CO_2 formed in ethanol condensation on

TABLE 2

Effects of Cu- and K-loading on Ethanol Consumption and Product Formation on Mg_5CeO_x

		Rates of formation					
		Ethanol dehydrogenation		Acetone + 2-Propanol		Butyraldehyde + 1-Butanol	
Cu (wt%)	K (wt%)	Areal rate r_1[a]	Turnover rate r_1[b]	Areal rate r_2[c]	Turnover rate r_2[d]	Areal rate r_3[c]	Turnover rate r_3[d]
0	0	4.0×10^{-9}	—	7.5×10^{-11}	7.9×10^{-5}	2.8×10^{-11}	2.9×10^{-5}
0	0.8	3.4×10^{-9}	—	9.7×10^{-11}	5.6×10^{-5}	1.6×10^{-10}	9.4×10^{-5}
7	0.1	3.6×10^{-7}	0.24	3.0×10^{-9}	2.2×10^{-3}	4.5×10^{-10}	3.4×10^{-4}
7	1.0	2.4×10^{-7}	0.23	4.3×10^{-9}	1.8×10^{-3}	7.6×10^{-10}	3.2×10^{-4}
49	1.2	9.4×10^{-7}	0.24	4.4×10^{-8}	1.0×10^{-2}	1.2×10^{-9}	2.8×10^{-4}

[a] r_1 is the rate of ethanol consumption, in mol/m^2 total · s.
[b] Turnover rates per Cu surface atom, in s^{-1}.
[c] r_2 and r_3 are the rates of product formation, in mol/m^2 $MgCeO_x$ · s.
[d] Turnover rates per accessible site from $^{13}CO_2/^{12}CO_2$ in mol C_2H_5OH/mol basic site · s; basic sites measured by $^{13}CO_2/^{12}CO_2$ isotopic switch method (13, 38).

base-catalyzed dehydrogenation reactions on Mg_5CeO_x. Dehydrogenation rates were much higher on $Cu_{0.5}Mg_5CeO_x$, 1.0 wt% K–$Cu_{0.5}Mg_5CeO_x$, and 1.2 wt% K–$Cu_{7.5}Mg_5CeO_x$ catalysts than on Mg_5CeO_x, suggesting that Cu sites catalyze ethanol dehydrogenation to acetaldehyde. The presence of K decreased areal ethanol dehydrogenation rates, because K decreased Cu dispersion. Ethanol dehydrogenation turnover rates (normalized by the number of exposed Cu atoms) on $Cu_{0.5}Mg_5CeO_x$, 1.0 wt% K–$Cu_{0.5}Mg_5CeO_x$, and 1.2 wt% K–$Cu_{7.5}Mg_5CeO_x$ catalysts were 0.24, 0.23, and 0.24 s^{-1}, respectively. Thus, ethanol dehydrogenation steps require exposed Cu atoms for the rate-determining step. Surface Cu atoms become unavailable for both N_2O decomposition and alcohol dehydrogenation when covered with K species or as Cu crystallites become larger. Dehydrogenation turnover rates were not affected by Cu crystallite size or by the titration of a fraction of the Cu surface with KO_x species.

Aldol coupling chain growth rates are lower on Mg_5CeO_x than on $Cu_{0.5}Mg_5CeO_x$ because of the lower acetaldehyde concentrations when Cu sites are not present. K increases the rate of base-catalyzed aldol coupling reactions to acetone and butyraldehyde (Table 2), even though steady-state acetaldehyde concentrations on $Cu_{0.5}Mg_5CeO_x$ and 1.0 wt% K–$Cu_{0.5}Mg_5CeO_x$ catalysts are similar on these two catalysts. Thus, it appears that the higher basic site densities determined by $^{13}CO_2/^{12}CO_2$ isotopic switch measurements indeed lead to higher rates of base-catalyzed aldol condensation reactions. The total rates of base-catalyzed aldol coupling reactions, when normalized by the number of accessible basic sites, are similar on $Cu_{0.5}Mg_5CeO_x$ (2.5×10^{-3}) and K–$Cu_{0.5}Mg_5CeO_x$ (2.2×10^{-3}). Aldol condensation rates on 1.2 wt% K–$Cu_{7.5}Mg_5CeO_x$ (49 wt% Cu, 0.047 Cu dispersion) are, however, much higher than on catalysts with lower Cu content, even though the density of basic sites is similar on these two samples. The difference in condensation rates suggests that Cu sites are involved in rate-determining steps required for condensation reactions, even though such Cu sites are present in sufficient number to ensure ethanol-acetaldehyde thermodynamic equilibrium. The lower aldol coupling chain growth reaction rates observed on Cu-free catalysts, which is caused not only by the low concentration of required acetaldehyde intermediates but also by the absence of Cu sites required in condensation steps, is consistent with this proposal.

A sequential reaction scheme, where ethanol dehydrogenates to form gas phase acetaldehyde, which then undergoes self-condensation reactions into products, is not considered, because it is not consistent with the sharp initial increase in product site-yield curves (Fig. 1). On Cu containing catalysts, the steady-state acetaldehyde concentrations are similar. The effect of copper suggests a bifunctional mechanism for aldol condensation on metal-promoted basic oxides; this mechanistic proposal is discussed in detail below.

The proposed mechanism involves the initial dissociative adsorption of ethanol on MgO to form ethoxide and hydrogen species (43, 44). Hydrogen species can then be removed by migration to Cu sites, recombination with another hydrogen adatom, and desorption as H_2:

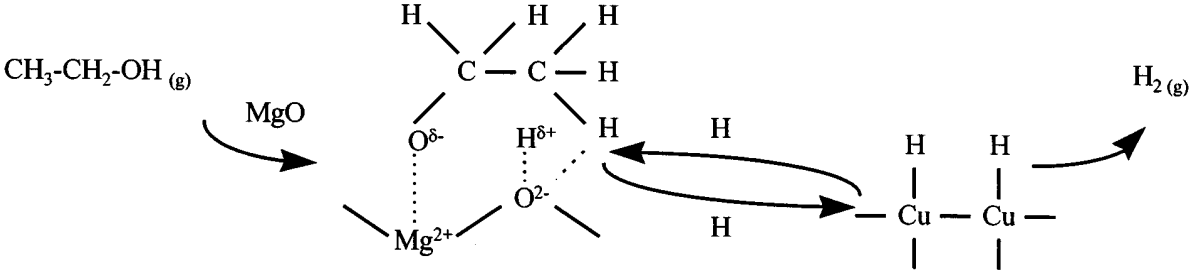

Additional C–H bond cleavage events in ethoxide species can then occur and the hydrogen atoms formed are transferred to oxygen ions and form surface acetaldehydic species:

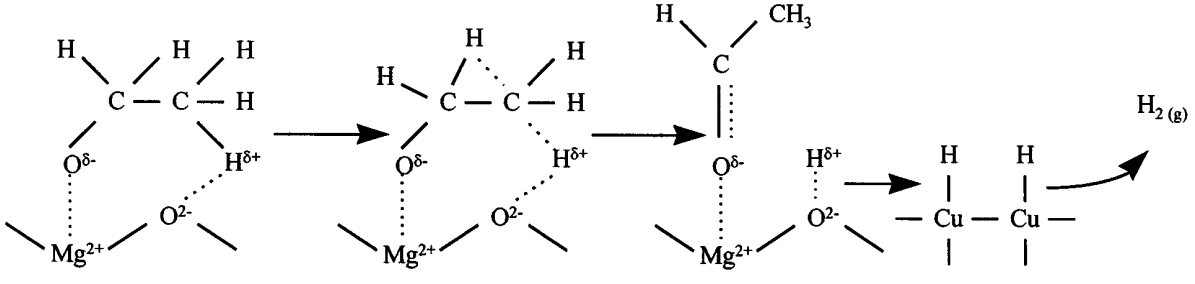

In this scheme, hydrogen atoms migrate from basic to Cu sites and recombine to form H_2. As a result, basic oxygen sites become available for another hydrogen abstraction step. H–H recombination rates increase with increasing ratio of surface Cu atoms to basic sites, which is 0.31 on K–$Cu_{7.5}Mg_5CeO_x$ and 0.07 on K–$Cu_{0.5}Mg_5CeO_x$, at similar basic

site density. The high ratio of Cu to basic oxide surface area on K–$Cu_{7.5}Mg_5CeO_x$ leads to higher aldol-condensation rates than on catalysts with lower ratios, without a detectable effect on the (equilibrium) concentration of acetaldehyde.

Adsorbed acetaldehyde species can desorb as acetaldehyde or react with other surface species to form aldol condensation products:

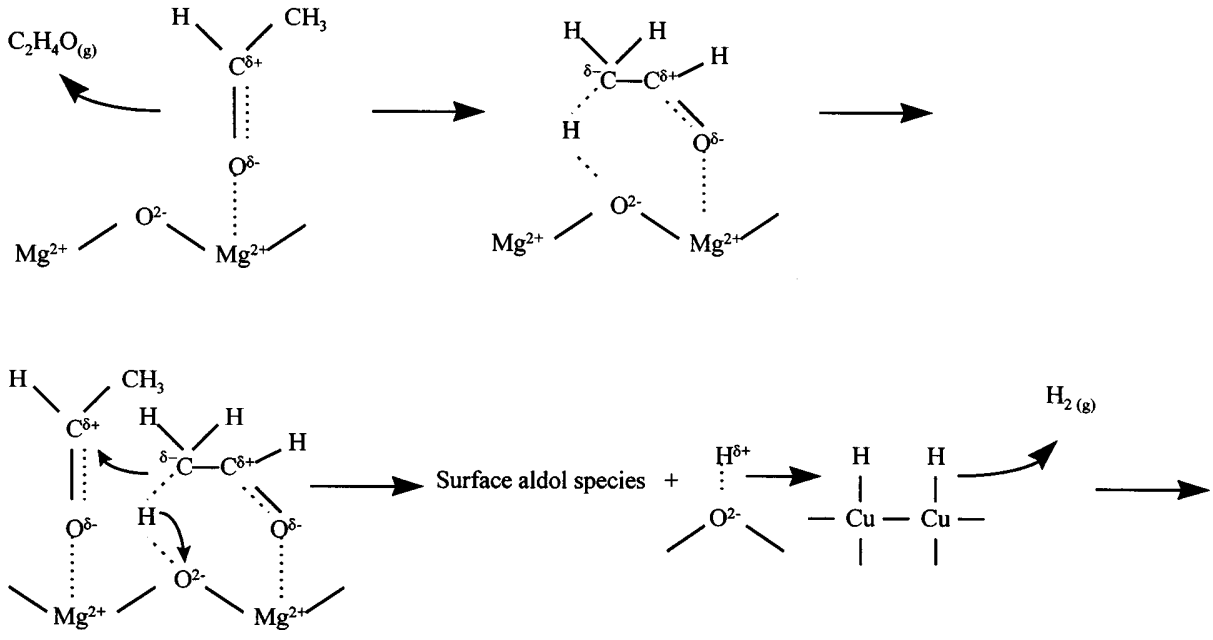

Surface aldol species can undergo condensation reactions via the pathways shown in Scheme 4. In these reactions, the presence of Cu sites increases the rate of hydrogen removal and reintroduction and provides the hydrogen atoms required for hydrogenation of unsaturated aldehyde species (steps IV, VII, and XII, Scheme 4). The non-zero initial slopes of acetone and n-butyraldehyde turnover-time plots (Fig. 1) are consistent with the direct condensation of ethanol reactants. These bifunctional condensation pathways are qualitatively similar in kinetic structure to those proposed for bifunctional C–H activation of alkanes on cation-modified zeolites (45–47).

The ratio of C_3 to C_4 oxygenates measured on the different catalysts gives the selectivity of the decomposition of keto species to form acetone (Scheme 4, step X) compared to aldol dehydration–hydrogenation of such species to form n-butyraldehyde (Scheme 4, steps III and IV). On Cu-free catalysts this ratio is <3, and the total condensation rate is $\sim 10^{-10}$ mol/m^2-s. At high Cu concentrations, the C_3/C_4 selectivity ratio increases to 37, while the total condensation rate increases to $\sim 10^{-8}$ mol/m^2-s. Thus, in addition to increasing the surface concentration of aldol species via removal of adsorbed hydrogen atoms, Cu appears to enhance hydrogen transfer steps required for enol-keto interconversion (Scheme 4, step VI); as a result, Cu sites increase the concentration of keto species and the rate of step X (Scheme 4).

3.3. Reactions of Acetaldehyde

In Section 3.2, we proposed that condensation reactions could proceed (i) via direct reactions of ethanol without the intermediate formation of gas phase acetaldehyde molecules, or (ii) through consecutive reactions including the formation of gas-phase acetaldehyde, with zero order kinetics in acetaldehyde concentration. In order to test the second possibility, catalytic activity and product yields for acetaldehyde reactions on 1.0 wt% K–$Cu_{0.5}Mg_5CeO_x$ were measured at several acetaldehyde pressures.

Acetone and crotonaldehyde are the predominant products of acetaldehyde reactions (Fig. 2). Carbon dioxide, n-butyraldehyde, and 2-pentanone were also detected in small concentrations among reaction products. Ethanol forms by hydrogenation of acetaldehyde using H-adatoms formed in C–H activation steps or H_2 molecules desorbed by Cu sites after C–H activation. Aldol-type condensation of acetaldehyde forms crotonaldehyde, which then hydrogenates to form n-butyraldehyde. Acetaldehyde can also polymerize to give dimers and trimers (Scheme 5) and/or by sequential aldol condensations leading to high molecular weight aldehydes (48). These polymeric species are likely to remain on the catalyst surface and may account for the poor overall mass balances observed in these experiments

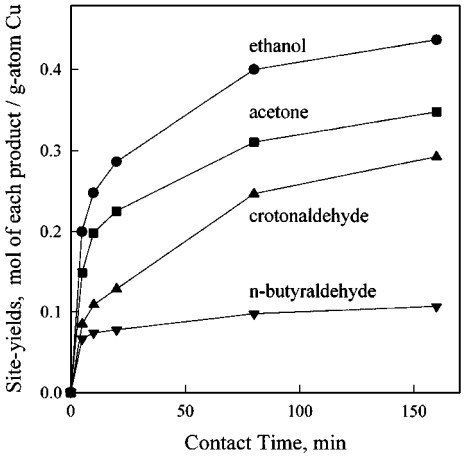

FIG. 2. Acetaldehyde reactions. Site yields as a function of contact time on 1.0 wt% K–$Cu_{0.5}Mg_5CeO_x$ (573 K, 101.3 kPa total pressure, 8.0 kPa acetaldehyde pressure, balance He).

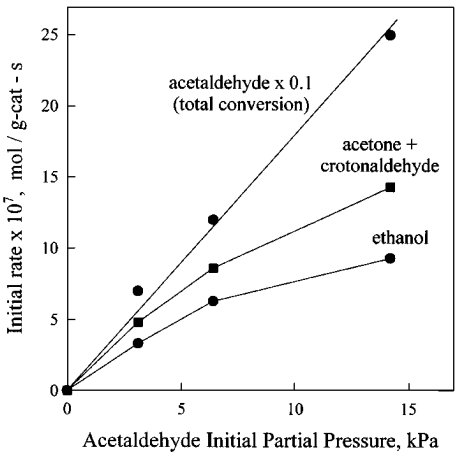

FIG. 3. Acetaldehyde reactions. Effect of the acetaldehyde initial partial pressure over the initial rates. Acetaldehyde conversion as a function of contact time on 1.0 wt% K–$Cu_{0.5}Mg_5CeO_x$ (573 K, 101.3 kPa total pressure, 3–15 kPa acetaldehyde pressures, balance He).

(carbon selectivity totals less than 45%). Hydrogen is also produced by decomposition of the formaldehyde formed in retro-aldol reactions leading to acetone (Scheme 4).

Initial reaction rates at different initial partial pressures of acetaldehyde are shown in Fig. 3. Condensation, hydrogenation, and total conversion rates are approximately first order in acetaldehyde concentration. These results show that the initial reaction nonzero slope for condensation products in ethanol reactions (Fig. 1) cannot reflect zero-order kinetics for aldehyde condensation. Instead, it suggests that direct reactions of ethanol account for a significant fraction of the condensation products formed from ethanol reactants.

Figure 4 shows the molar ratio of ethanol to acetone and of C_4 oxygenates (crotonaldehyde and n-butyraldehyde) to acetone among the reaction products and the initial condensation rates for acetaldehyde reactions on K–$Cu_yMg_5CeO_x$ catalysts. Aldol coupling chain growth rates increase with increasing copper surface area. The increase, however, is less pronounced than for reactions of ethanol. These results show that Cu sites also increase rates of C–H bond activation in acetaldehyde.

Acetone is a condensation product, while ethanol is a hydrogenation product. The molar ratio between ethanol/acetone is a measurement of the catalyst ability to remove H-atoms from the surface by recombinative desorption compared to its ability to catalyze condensation reactions. On Mg_5CeO_x catalysts, ethanol is produced selectively over acetone. The catalyst surface is saturated with H-atoms from the abstraction of α-hydrogens from acetaldehyde on basic sites. Without Cu, it is more probable

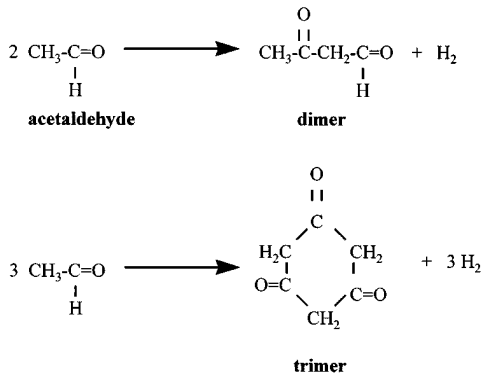

SCHEME 5. Formation of dimer and trimer compounds from acetaldehyde.

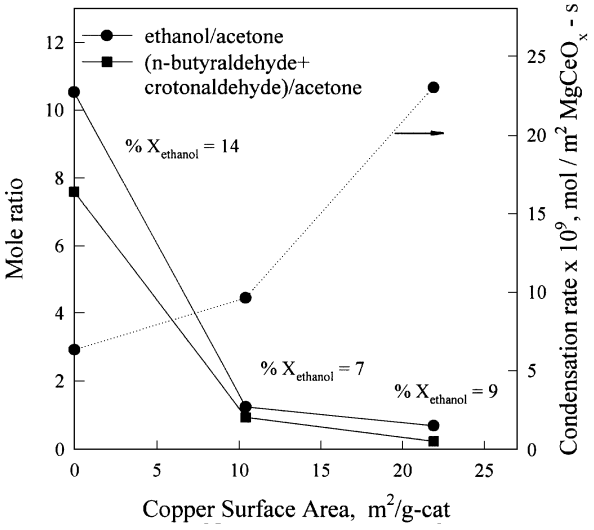

FIG. 4. C_2 to C_3 and C_4 to C_3 molar ratios on acetaldehyde reactions and initial acetaldehyde condensation rates as a function of Cu surface area on K–$Cu_yMg_5CeO_x$ catalysts (573 K, 101.3 kPa total pressure, 6.6 kPa acetaldehyde, balance He).

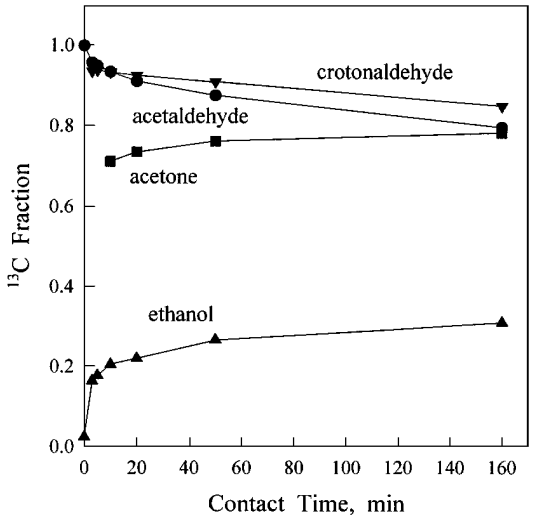

FIG. 5. ^{13}C-content in reactants and reaction products ($^{13}C_2H_4O$–C_2H_5OH–H_2 reaction mixtures on 0.8 wt% K–Mg_5CeO_x) (523 K, 101.3 kPa total pressure, 2.9 kPa acetaldehyde pressure, 1.1 kPa ethanol pressure, 2.9 kPa hydrogen pressure, balance He).

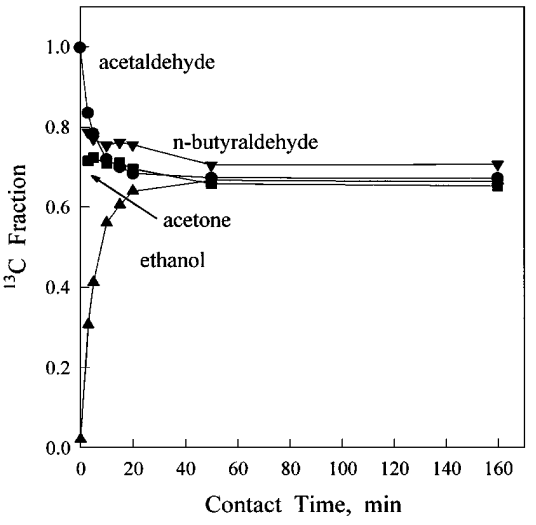

FIG. 7. ^{13}C-content in reactants and reaction products ($^{13}C_2H_4O$–C_2H_5OH–H_2 reaction mixtures on 1.2 wt% K–$Cu_{7.5}Mg_5CeO_x$) (523 K, 101.3 kPa total pressure, 2.9 kPa acetaldehyde pressure, 1.1 kPa ethanol pressure, 2.9 kPa hydrogen pressure, balance He).

that the H-atoms are used to hydrogenate acetaldehyde to ethanol. When Cu sites are present, ethanol selectivity decreases markedly because these H-atoms recombine to form H_2. On the other hand, acetone is formed selectivity on Cu-containing catalysts instead of n-butyraldehyde or crotonaldehyde. This shows that reverse aldol reaction steps from C_4 intermediates (Scheme 4) become less likely as Cu is introduced into the catalysts.

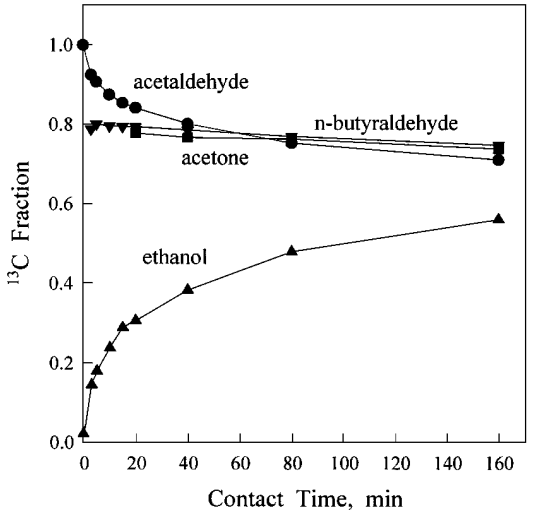

FIG. 6. ^{13}C-content in reactants and reaction products ($^{13}C_2H_4O$–C_2H_5OH–H_2 reaction mixtures on 1.0 wt% K–$Cu_{0.5}Mg_5CeO_x$) (523 K, 101.3 kPa total pressure, 2.9 kPa acetaldehyde pressure, 1.1 kPa ethanol pressure, 2.9 kPa hydrogen pressure, balance He).

3.4. Reactions of C_2H_5OH/$^{13}C_2H_4O$ Mixtures

As discussed in Section 3.2, it appears that ethanol undergoes condensation reactions directly, without requiring its intermediate conversion to gas phase acetaldehyde. Also, condensation rates increase with increasing acetaldehyde concentration. Chung *et al.* (49), using $CH_3{}^{13}CH_2OH/C_2O_4H$ mixtures on Cu/ZnO catalysts, showed that acetone can be produced by C–C bond cleavage in C_4 species formed from two aldehydic species and n-butyraldehyde by C–O bond cleavage in C_4 species formed from ethanol and acetaldehyde. In order to examine the role of ethanol and to detect available direct pathways for ethanol condensation, competitive reactions between $^{12}C_2H_5OH$ and $^{13}C_2H_4O$ were carried out on 0.8 wt% K–Mg_5CeO_x, 1.0 wt% K–$Cu_{0.5}Mg_5CeO_x$, and 1.2 wt% K–$Cu_{7.5}Mg_5CeO_x$ catalysts. The carbon-13 contents in reactants and products as a function of contact time are shown in Figs. 5, 6, and 7.

On all catalysts, the ^{13}C-content in both ethanol and acetaldehyde changes with contact time, as the products reach chemical and isotopic equilibrium. The rate of ethanol-acetaldehyde equilibration is much higher on 1.2 wt% K–$Cu_{7.5}Mg_5CeO_x$ than on the other two catalysts. When copper is present, hydrogenation–dehydrogenation reactions occur more rapidly, in agreement with the results shown in Section 3.2. On Cu-free catalysts (Fig. 5), the ^{13}C-content in both ethanol (30%) and acetaldehyde (80%) reach values that differ markedly from those predicted at isotopic equilibrium (70%). This is consistent with the rapid deactivation observed during ethanol reactions on Cu-free catalysts (Sections 3.2, 3.3).

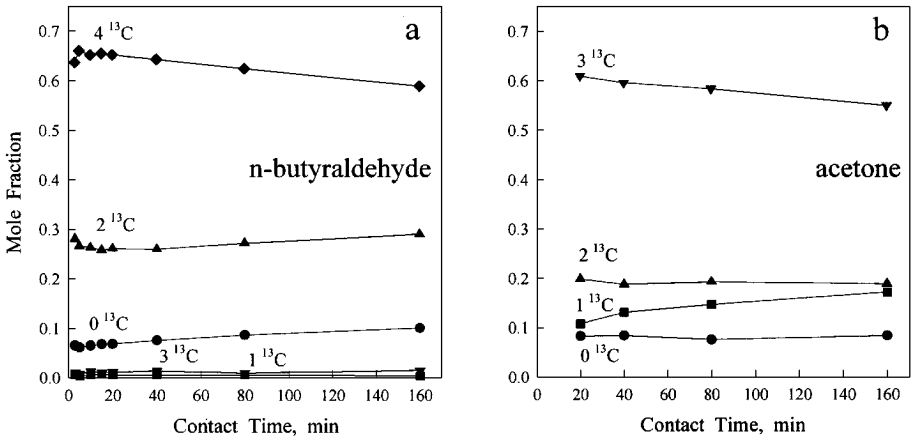

FIG. 8. ^{13}C-distribution of products in $^{13}C_2H_4O$–C_2H_5OH–H_2 reactions on 1.0 wt% K–$Cu_{0.5}Mg_5CeO_x$ as a function of contact time (523 K, 101.3 kPa total pressure, 2.9 kPa acetaldehyde pressure, 1.1 kPa ethanol pressure, 2.9 kPa hydrogen, balance He).

The ^{13}C-distributions in the products of $^{13}C_2H_4O$–C_2H_5OH–H_2 mixtures on 1.0 wt% $Cu_{0.5}Mg_5CeO_x$ are shown in Fig. 8. The ^{13}C-content in condensation products changes slightly with contact time, but the isotopic content in ethanol and acetaldehyde (Figs. 6 and 8) change significantly. These data may reflect (i) the rapid formation of surface polymer species from the starting mixture and the subsequent formation of all products *only* from this surface polymer pool or (ii) a similar reactivity of ethanol and acetaldehyde in condensation products, leading to products that contain the (constant) average ^{13}C-content within the remaining reactant pool. The first possibility is unlikely because the decomposition of surface polymer species would lead to C_1, C_2, C_3, etc. species and not only n-butyraldehyde and acetone. The second explanation seems more plausible. On Cu-containing catalysts, hydrogenation–dehydrogenation steps (ethanol = acetaldehyde + H_2) are fast and the ^{13}C-content in acetone and n-butyraldehyde extrapolated to zero contact time is about 80%. If these products formed only from acetaldehyde, they should contain only ^{13}C, and if they formed only from ethanol, they should be unlabeled. This 80% value shows that ethanol and acetaldehyde contribute to products in proportion to their concentration in the reactant pool. The ^{13}C-composition of the reactant mixture is 73%, which is less than the 80% observed for ^{13}C-content in products. The ^{13}C-contents in products decreases slightly with contact time, similar to the ^{13}C-content decrease observed in acetaldehyde (Figs. 6 and 8). These findings suggest that product formation rates from acetaldehyde are slightly higher than from ethanol, but that direct condensation of ethanol occurs readily at these reaction conditions.

Table 3 shows the ^{13}C-content in n-butyraldehyde formed on 1.0 wt% K–$Cu_{0.5}Mg_5CeO_x$ and in crotonaldehyde formed on 0.8 wt% K–Mg_5CeO_x, obtained by extrapolating to zero conversion. Table 3 also shows the predicted binomial ^{13}C distributions when n-butyraldehyde forms only from ethanol, only from acetaldehyde, or from both ethanol and acetaldehyde with equal probability. These data (Fig. 8, Table 3) suggest that n-butyraldehyde and acetone are formed from both reactants (ethanol and acetaldehyde). In contrast, the ^{13}C-content in crotonaldehyde formed on 0.8 wt% K–Mg_5CeO_x at relatively low contact times (Table 3) shows that it is produced predominantly from acetaldehyde.

Ethanol adsorbs dissociatively on MgO to form surface ethoxide and hydrogen species (43, 44). In the absence of the Cu sites that provide a H–H recombination function, surface ethoxide and hydrogen recombine preferably and desorb as ethanol, instead of remaining as adsorbed ethoxide species that then lose a β-H to give surface aldehydic

TABLE 3

^{13}C-distribution of Prodcuts (mole fraction) in $^{13}C_2H_4O$–C_2H_5OH–H_2 reactions on 1.0 wt% $Cu_{0.5}Mg_5CeO_x$ and 0.8 wt% K–Mg_5CeO_x

Number of ^{13}C	Predicted[a] Ethanol	Predicted[a] Acetaldehyde	Predicted[a] Both	n-Butyraldehyde[b] 1.0 wt% $Cu_{0.5}Mg_5CeO_x$	Crotonaldehyde[b] 0.8 wt% K–Mg_5CeO_x
0	1.00	0	0.08	0.07	0.02
1	0	0	0	0	0
2	0	0	0.39	0.30	0.12
3	0	0	0	0	0
4	0	1.00	0.53	0.63	0.86

Note. 523 K, 101.3 kPa total pressure, 2.9 kPa acetaldehyde pressure, 1.1 kPa ethanol pressure, 2.9 kPa hydrogen, balance He.

[a] Calculated by assuming the n-butyraldehyde or crotonaldehyde are formed exclusively from ethanol, or from acetaldehyde or from both with identical probability.

[b] Experimental values extrapolated to zero conversion.

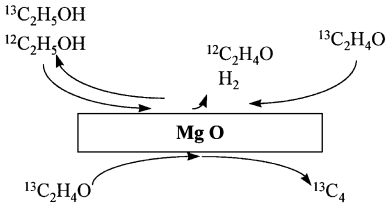

SCHEME 6. Competitive reactions of $^{13}C_2H_4O$–C_2H_5OH–H_2 mixtures.

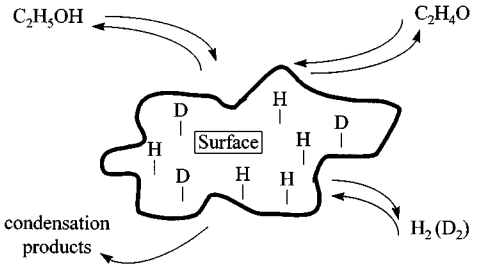

SCHEME 7. Ethanol reactions and hydrogen removal steps.

species and condense with other surface species. Some H-atoms are used to hydrogenate adsorbed aldehydic species, which leave the surface as labeled ethanol (Scheme 6). In this situation, it is more likely that two adsorbed acetaldehyde molecules react with each other leading to labeled aldol intermediates.

These isotopic tracer studies of $^{12}C_2H_5OH$–$^{13}C_2H_4O$ mixtures suggest that condensation reaction can proceed via two parallel pathways: direct reactions of ethanol without the intermediate formation of gas phase acetaldehyde molecules and sequential dehydrogenation to form acetaldehyde followed by condensation steps (Scheme 6). These results show that "dehydrogenation" and condensation steps of ethanol can occur on the same type of active site, an acid-base site pair on MgO. This proposal is consistent with the promoting effect of Cu on condensation rates, with the initial non-zero slope of product concentration curves observed in ethanol reactions, and with the ^{13}C content in the condensation products of $^{12}C_2H_5OH$–$^{13}C_2H_4O$ mixtures.

3.5. Reactions of C_2H_5OH/D_2 Mixtures

As mentioned above, ethanol reactions on K–$Cu_yMg_5CeO_x$ lead to acetaldehyde, acetone, and n-butyraldehyde as predominant products. Acetaldehyde and ethanol condensation reactions occur on basic sites, but condensation rates increase with increasing density of Cu surface atoms (Table 2). Hydrogen abstraction steps (involved in condensation reactions) appear to be limited by the rate of hydrogen removal via recombinative desorption. This desorption process occurs rapidly on Cu surface atoms, but it is slow on metal-free MgO or $MgCeO_x$. Hydrogen migration and recombinative desorption on Cu sites can then increase aldol condensation rates by removing a surface bottleneck that tends to reverse the steps that form unsaturated aldol-type species required for chain growth.

In order to probe the reversibility of hydrogen adsorption-desorption pathways (Scheme 7), ethanol reactions were carried out in the presence of gas phase D_2. The recombinative hydrogen disposal steps can be quasi-equilibrated or irreversible steps during ethanol coupling reactions. Quasi-equilibrated desorption steps would result in the formation of reaction products and reactants containing a statistical mixture of D-atoms from D_2 and H-atoms from ethanol. The deuterium content in reaction products, therefore, measures the rate of communication between the surface and gas phase hydrogen pools. In contrast, irreversible recombinative desorption steps would lead to reaction products containing predominantly protium, because the slow communication between gas phase (D_2) and surface hydrogen pool leads to predominant presence of protium atoms formed in C–H activation steps on the catalyst surface.

The role of Cu sites in ethanol reactions was examined by measuring the initial rates of D-atom incorporation into unreacted ethanol and into reaction products. These data are shown as a function of contact time in Fig. 9 on 0.8 wt% K–Mg_5CeO_x, 1.0 wt% K–$Cu_{0.5}Mg_5CeO_x$, and 1.2 wt% K–$Cu_{7.5}Mg_5CeO_x$ catalysts. The initial rates of incorporation of deuterium into ethanol, acetaldehyde, and acetone as a function of Cu surface area were calculated from the initial slopes in Fig. 9 and the results for K–$Cu_yMg_5CeO_x$ catalysts are summarized in Table 4. The distribution of deuterium atoms in unreacted ethanol, acetaldehyde, and acetone products of ethanol/D_2 mixtures at different contact times are shown in Fig. 10.

The rate of appearance of deuterium in unreacted ethanol and in reaction products (Fig. 9 and Table 4) increases with increasing Cu content on Mg_5CeO_x catalysts. The deuterium fraction is much lower on Mg_5CeO_x

TABLE 4

Reactions of C_2H_5OH/D_2 Mixtures

Catalyst	Cu surface area (m^2/g_{cat})	Ethanol		Acetaldehyde		Acetone	
		r_D[a]	r_t[b]	r_D[a]	r_t[b]	r_D[a]	r_t[b]
Mg_5CeO_x	0	4.5	78.2	1.4	57.9	0.02	0.38
$Cu_{0.5}Mg_5CeO_x$	10.4	129	514	200	469	6.7	5.6
$Cu_{7.5}Mg_3CeO_x$	21.9	925	683	601	585	78	27

Note. Effect of Cu Surface Area on the Initial Rates of Incorporation of Deuterium into Unreacted Ethanol and Products.

[a] r_D is the rate of deuterium incorporation in unreacted ethanol and $\times 10^7$, in mol D_2/g-cat · s.

[b] r_t is the rate of ethanol consumption or product formation $\times 10^7$, in mol/g-cat · s.

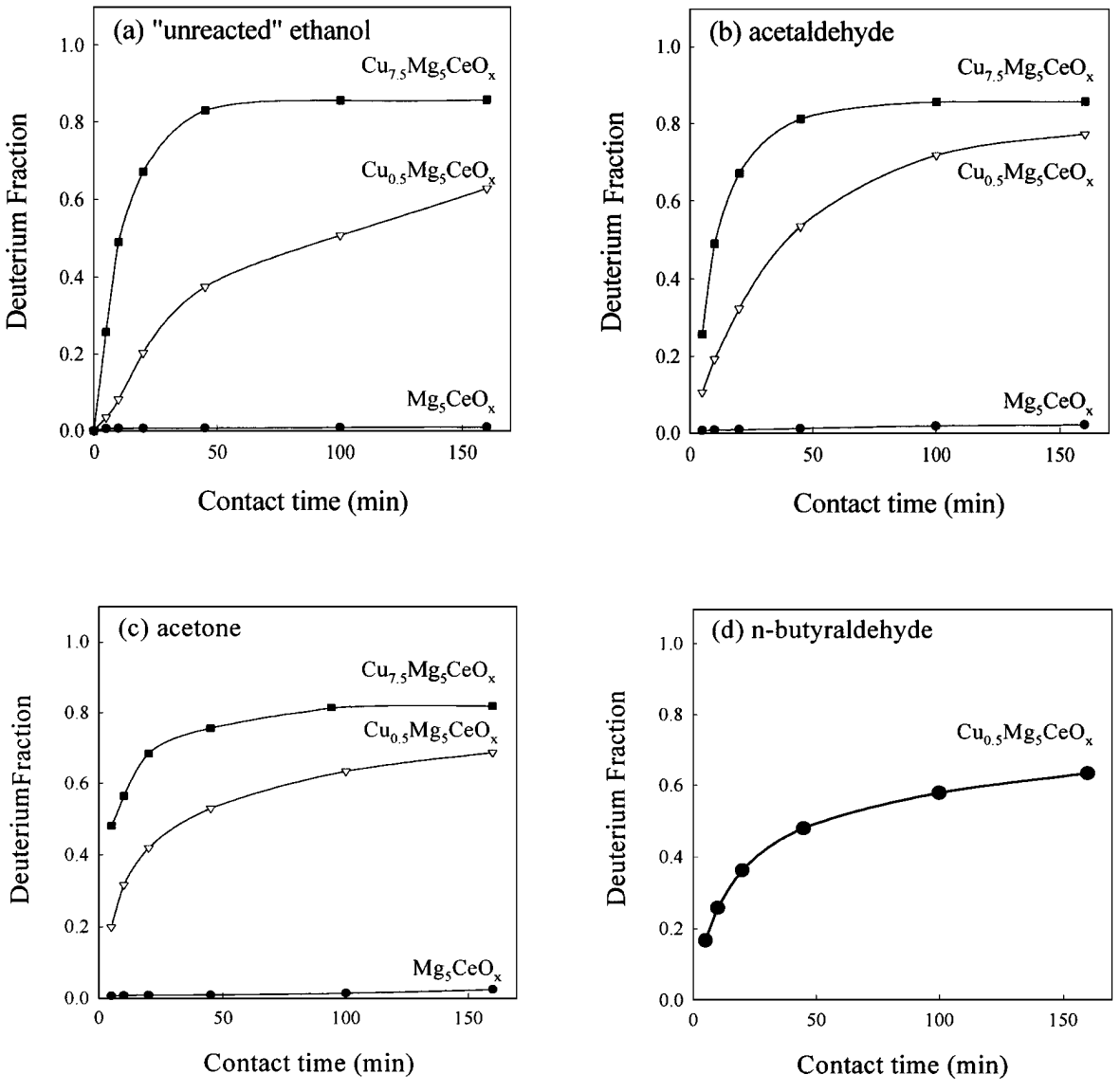

FIG. 9. Deuterium fraction in unreacted ethanol (a) and in acetaldehyde (b), acetone (c), and n-butyraldehyde (d) formed from ethanol/D_2 mixtures (~20% H, ~80% D) on K–$Cu_yMg_5CeO_x$ catalysts (573 K, 101.3 kPa total pressure, 3.6 kPa ethanol pressure, 27 kPa D_2 pressure, balance He).

than on Cu-containing catalysts, suggesting that Cu sites increase the rate of communication between surface and gas phase hydrogen pools by providing a site for dissociative D_2 chemisorption and for recombinative desorption of H-atoms formed in C–H bond activation steps occurring on basic sites.

At short contact times (Fig. 10), gas phase molecules (and adsorbed species in equilibrium with them) have relatively low deuterium contents. Singly-deuterated species are the most abundant, suggesting that gas phase D_2 contributes weakly to the surface hydrogen pool. This surface hydrogen pool contains predominantly H-atoms formed by C–H bond activation steps required in ethanol dehydrogenation reactions. The deuterium content in reactants and products increases with increasing contact time. All deuterium distributions are binomial, suggesting that every C–H (and O–H) bond is broken and reformed several times during the formation of one product molecule (while the precursor molecule remains adsorbed on the surface) or that a desorbed molecule returns to the surface and exchanges sequentially with the surface H–D pool. The latter process leads to the observed increase in deuterium content with contact time.

Initial rates of ethanol dehydrogenation and of deuterium incorporation into ethanol (in ethanol/D_2 mixtures) on K–$Cu_yMg_5CeO_x$ catalysts are shown in Fig. 11 as a function of Cu surface area. The initial rate of ethanol dehydrogenation increases linearly with Cu surface area

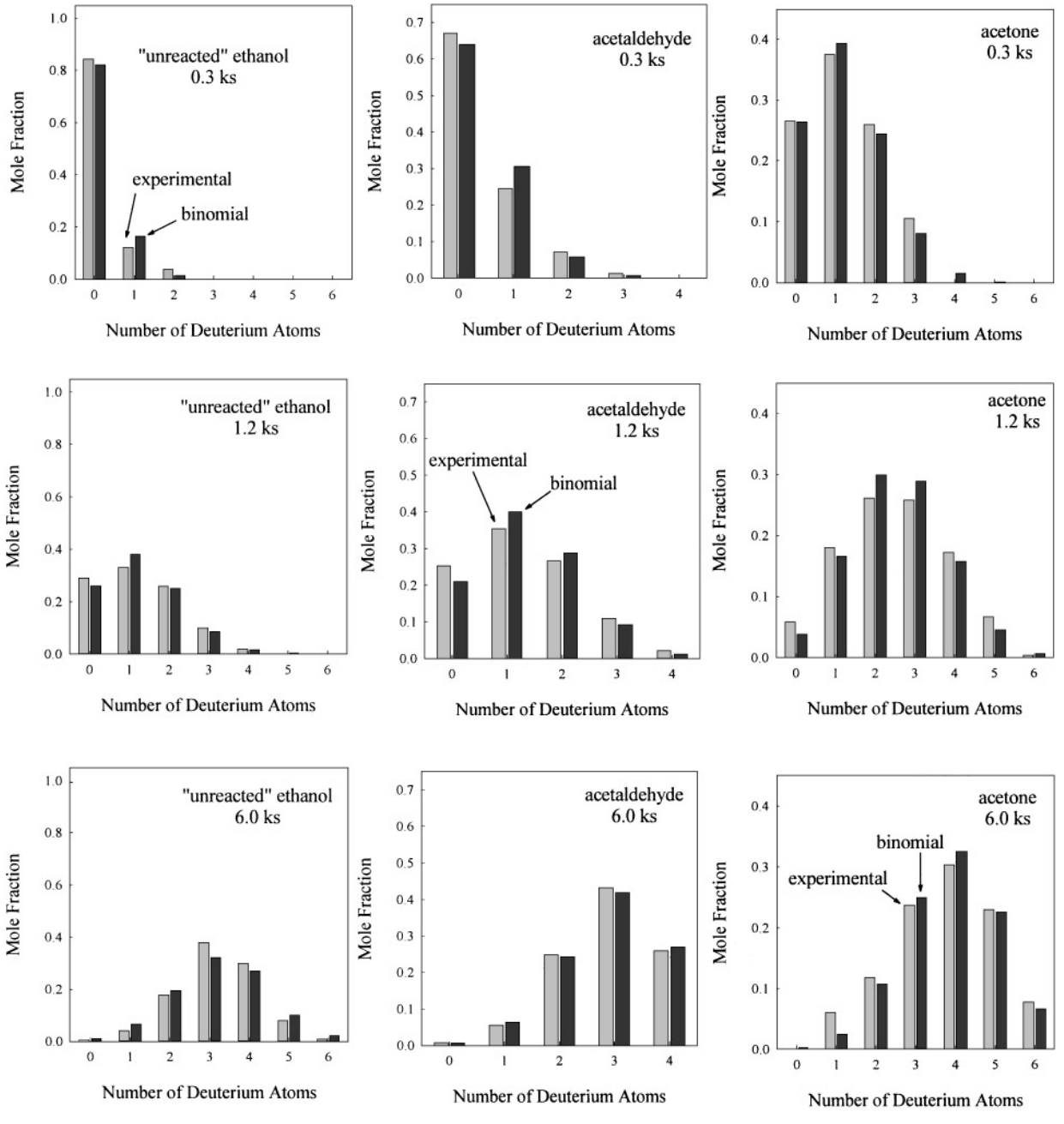

FIG. 10. Reactions of C_2H_5OH/D_2 mixtures on 1.0 wt% $K–Cu_{0.5}Mg_5CeO_x$ catalyst. Deuterium distributions in unreacted ethanol and acetaldehyde and acetone products at various contact times (0.3 ks, 1.2 ks, 6.0 ks) (573 K, 101.3 kPa total pressure, 3.6 kPa ethanol pressure, 27 kPa D_2 pressure, balance He).

(measured by N_2O decomposition methods); therefore, dehydrogenation turnover rates are not affected by Cu crystallite size and involve a rate-determining step occurring on Cu surface atoms. At similar steady-state acetaldehyde concentrations, condensation rates to form acetone and n-butyraldehyde also increase with increasing Cu surface area (Fig. 11), even though basic site densities measured by CO_2 isotopic switch methods are very similar on these catalysts (Table 1). Therefore, Cu metal sites are also required for the rate-determining step in condensation reactions. If hydrogen removal is rate-determining in ethanol dehydrogenation and condensation reactions, Cu may provide the required site for the recombinative desorption of H-atoms formed in C–H bond activation reactions on MgO acid-base sites. The removal of H species from basic oxygen atoms on MgO surfaces frees such sites for the required activation of the next C–H bond. The increase in the rate of deuterium incorporation into unreacted ethanol with increasing amount

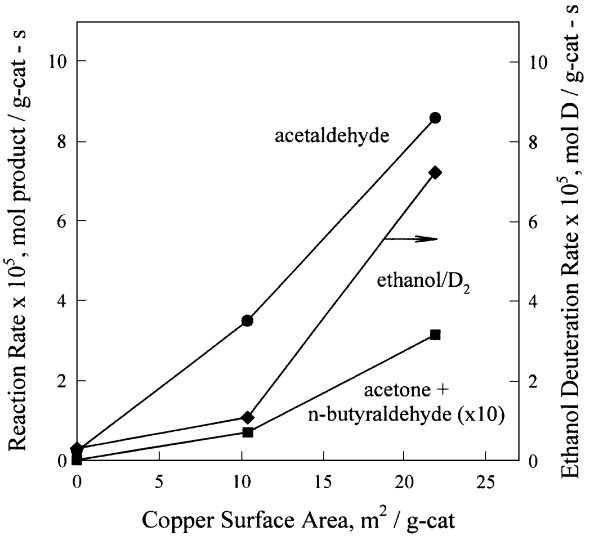

FIG. 11. Initial rates of ethanol dehydrogenation and condensation and of incorporation of deuterium into ethanol (in ethanol/D_2 mixtures) as a function of Cu surface area on K–$Cu_yMg_5CeO_x$ catalysts (573 K, 101.3 kPa total pressure, 3.7 kPa ethanol (27 kPa D_2), balance He).

of Cu surface atoms is consistent with faster rates of H_2 adsorption–desorption steps when Cu is present. When H-atoms are not rapidly removed, they tend to reverse the C–H bond activation step that forms the unsaturated aldol-type species required for chain growth. As more Cu sites are introduced, hydrogen coverages decrease and the surface favors α-H abstraction surface steps.

3.6. Cross-Coupling Reactions of $^{13}CH_3OH/C_2H_4O$ and $^{13}CH_3OH/C_3H_6O$ Mixtures

Ethanol is a useful and simple probe molecule to test the role of individual components in metal–base bifunctional catalysts for isobutanol synthesis. Ethanol reactions, however, lead to acetone and n-butyraldehyde, which form only

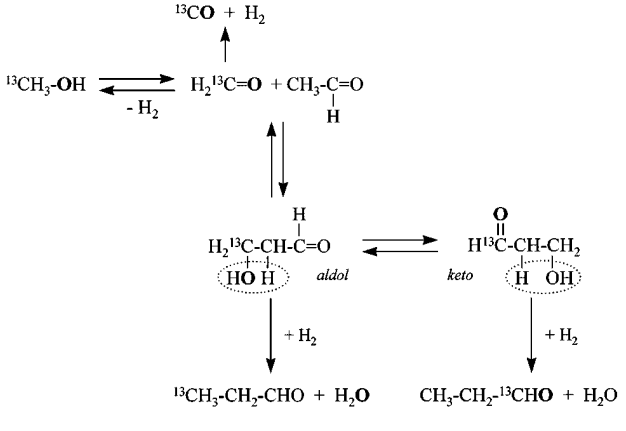

SCHEME 8. Reaction scheme of the interconversion of aldol and keto species.

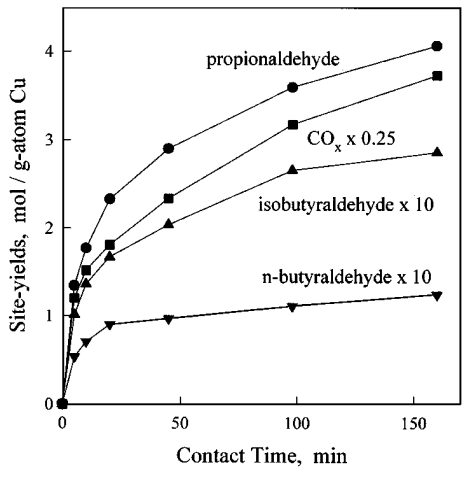

FIG. 12. Methanol-acetaldehyde reactions. Site yields as a function of contact time on 1.0 wt% K–$Cu_{0.5}Mg_5CeO_x$ (573 K, 101.3 kPa total pressure, 8.0 kPa methanol, 4.0 kPa acetaldehyde, balance He).

2-propanol and 1-butanol, after subsequent hydrogenation during CO/H_2 reactions. 2-Propanol and 1-butanol cannot, however, form isobutanol precursors (such as isobutyraldehyde and propionaldehyde) by condensation reactions during CO hydrogenation. ^{13}C-tracer studies of methanol reaction with acetaldehyde or propionaldehyde were carried out in order to examine reaction pathways that lead to the formation of the C_3 and C_4 oxygenate precursors required for isobutanol formation via aldol-type reactions of alcohols and aldehydes with methanol-derived C_1 species.

Cross-coupling site yields for $^{13}CH_3OH$–$^{12}C_2H_4O$ mixtures on $Cu_{0.5}Mg_5CeO_x$ are shown in Fig. 12. The initial rates (site-time yields per total 9-atom Cu) of methanol conversion were higher than that for the conversion of acetaldehyde to ethanol and to condensation products. The $^{13}CH_3OH$ component in the feed reacted predominantly to form ^{13}CO and H_2; this reaction reverses methanol synthesis because of the unfavorable methanol synthesis thermodynamics at atmospheric pressures (but not during

TABLE 5

^{13}C-Distribution in Products of $^{13}CH_3OH$–C_2H_4O Reactions on 1.0 wt% K–$Cu_{0.5}Mg_5CeO_x$

	Number of carbon-13				
	0	1	2	3	4
Carbon dioxide	11.4	88.6	—	—	—
Acetaldehyde	99.4	0.6	0	—	—
Ethanol	100	0	0	—	—
Propionaldehyde	4.4	91.6	4.1	0	—
n-Butyraldehyde	97.5	2.5	0	0	0
Isobutyraldehyde	0	10.1	70.3	20.6	0

Note. 573 K, 101.3 kPa total pressure, 8.0 kPa methanol, 4.0 kPa acetaldehyde, balance He.

CO hydrogenation at high pressures). The ethanol reaction product was predominantly unlabeled (Table 5) and it formed by hydrogenation of acetaldehyde using Cu sites and hydrogen produced via methanol decomposition.

Propionaldehyde contains predominantly one ^{13}C atom, suggesting that it is formed by condensation of acetaldehyde with reactive formyl or methoxy-type surface species or with gas phase formaldehyde derived from methanol. The analysis of the mass fragmentation pattern showed that the labeled carbon is present in either the CH_3 or CHO fragments of propionaldehyde. The methyl group contains 35% ^{13}C (at contact times of 2.7 h), suggesting that aldol condensation reactions can occur with retention of either one of the two oxygen atoms in aldol-keto species as proposed by Nunan *et al.* (7, 8). They used the term "oxygen retention reversal" to indicate the oxygen atom in the C_1 species (formaldehyde) remains in the final product, whereas in normal aldol condensation the oxygen of the growing intermediate remains in the final product. Both normal and oxygen retention reversal types of aldol condensation occurred on $K–Cu_yMg_5CeO_x$ catalysts. These types of reactions are caused by interconversion of aldol and keto species via H-transfer (Scheme 8).

Isobutyraldehyde contained predominantly two ^{13}C atoms, suggesting that it forms by condensation of propionaldehyde (with one ^{13}C) with a C_1 species formed from methanol (Table 5). The CO_2 product of $^{13}CH_3OH–{}^{12}C_2H_4O$ mixtures on $Cu_{0.5}Mg_5CeO_x$ was predominantly labeled and formed from ^{13}CO (via $^{13}CH_3OH$ decomposition) via water-gas shift reactions (Table 5). Acetone and n-butyraldehyde showed no significant ^{13}C-enrichment and they formed only by self-condensation reactions of acetaldehyde or ethanol, as also observed in reactions of pure ethanol (Scheme 4). This also accounts for the presence of small amounts of unlabeled CO_2. Only traces of labeled ethanol were detected among reaction products, suggesting that methanol coupling reactions, previously proposed as a route for C_1 to C_2 chain growth during higher alcohol synthesis (6), do not readily occur at these low pressures. In contrast with high-pressure CO hydrogenation conditions, our reaction conditions favor the decomposition of methanol and minimize its bimolecular chain-growth reactions.

These isotopic tracer studies are consistent with the sequence of steps shown in Scheme 9. Reverse aldol condensation reactions of aldol and keto species (formed from $^{13}C_1$ aldehyde-type intermediates and acetaldehyde) form 1-^{13}C labeled acetaldehyde, which in turn can lead to propionaldehyde with 2-^{13}C atoms, isobutyraldehyde with 3-^{13}C atoms, and traces of labeled n-butyraldehyde.

Reactions of propionaldehyde-^{13}C-methanol mixtures confirm these condensation pathways. These studies also show that aldol formation and dehydration–decarbonylation pathways are reversible. CO_x and H_2 (from methanol decomposition and water–gas shift reaction), isobutyraldehyde, 1-propanol, and methyl propionate were the main reaction products. Other products included methyl formate, 3-pentanone (from propionaldehyde self-condensation followed by decarboxylation), and 2-methyl-pentaldehyde (from propionaldeyde self-condensation). 2,2-dimethyl butyraldehyde (from cross coupling of isobutyraldehyde and C_1 species) was not observed, indicating that isobutyraldehyde (precursor to isobutanol) is a preferred end-product of chain growth reactions. Neither ethanol nor acetaldehyde were detected. Scheme 10 shows a reaction scheme for propionaldehyde-^{13}C-methanol coupling reactions consistent with the results presented in this section. Independent studies of alcohol reaction pathways during CO/H_2 reactions at high pressures [4.5 MPa, 573–593 K, $CO/H_2 = 1$] are also in agreement with the pathways reported here (50).

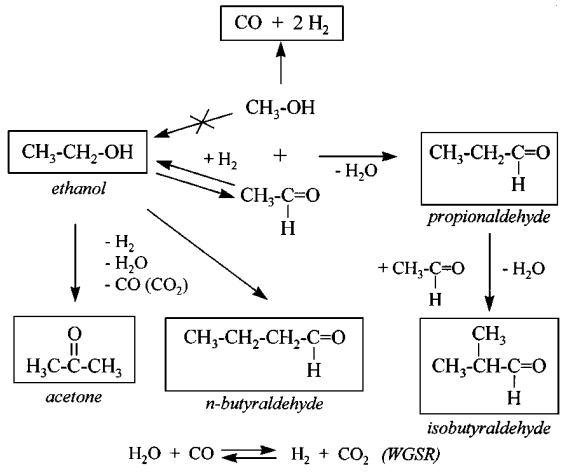

SCHEME 9. Reaction scheme for methanol-acetaldehyde reactions.

The results obtained from quantitative analysis of the isotopic content during propionaldehyde-^{13}C-methanol coupling reactions on 1.0 wt% $K–Cu_{0.5}Mg_5CeO_x$ are shown in Table 6. CO_2 molecules were predominantly labeled (88% ^{13}C) and formed from methanol-derived ^{13}CO via water–gas shift reactions. Unlabeled CO_2 was formed via decarboxylation reactions that also form 3-pentanone (Scheme 10). Propionaldehyde acquires some ^{13}C during reaction. The increase in the ^{13}C-content of propionaldehyde molecules as a function of contact time can be explained by Scheme 11. The proposed pathways include the formation of surface aldol species (from propionaldehyde and C_1 intermediates), keto-enol transformation (by intramolecular H-transfer) and reverse aldol condensation from the keto form, leading to propionaldehyde and C_1 species.

Isobutyraldehyde is predominantly labeled with one ^{13}C (Table 6), suggesting that it forms most frequently by cross-coupling reactions between ^{13}C-labeled methanol and propionaldehyde. Isobutyraldehyde with two ^{13}C forms by

TABLE 6

^{13}C-Distribution in Reactants and Products of $^{13}CH_3OH$–C_3H_6O Reactions on 1.0 wt% K–$Cu_{0.5}Mg_5CeO_x$

Time (min)	0	5	10	20
Propionaldehyde				
0	1.000	0.999	0.998	0.996
1	0.000	0.001	0.002	0.004
2	0.000	0.000	0.000	0.000
3	0.000	0.000	0.000	0.000
% ^{13}C	0.000	0.000	0.001	0.002
Isobutyraldehyde				
0		0.000	0.000	0.000
1		0.978	0.958	0.941
2		0.034	0.054	0.069
3		0.000	0.000	0.000
4		0.000	0.000	0.000
% ^{13}C		0.252	0.243	0.262
Methyl propionate				
0			0.033	0.023
1			1.025	0.988
2			0.000	0.000
3			0.002	0.000
4			0.000	0.000
% ^{13}C			0.228	0.242

Note. 573 K, 101.3 kPa total pressure, 7.7 kPa methanol, 3.5 kPa propionaldehyde, balance He.

aldol condensation reactions of labeled methanol ($^{13}C_1$ aldehyde-type intermediate) with singly-labeled propionaldehyde formed by reverse aldol condensation reactions. Methyl propionate also contains predominantly one ^{13}C, showing that it forms via reactions of methanol (methoxide) with propionaldehyde by Tischenko-type reactions (34). Both carbon atoms of methyl formate were labeled, indicating that it is formed from two molecules of methanol.

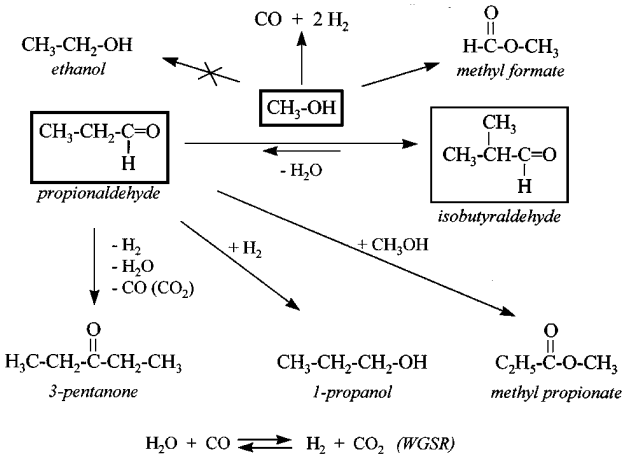

SCHEME 10. Reaction scheme for methanol–propionaldehyde reactions.

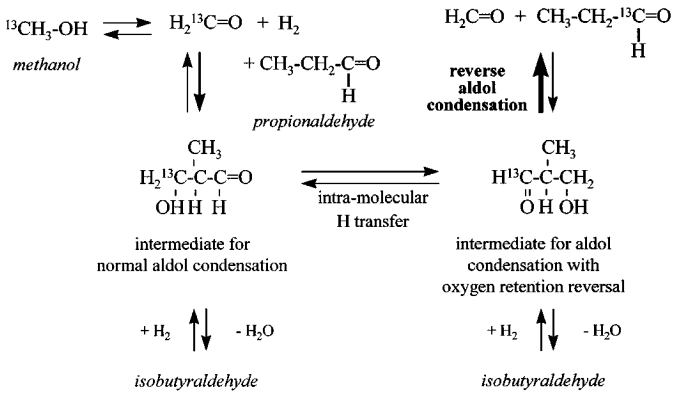

SCHEME 11. Reaction scheme of the labeled propionaldehyde production.

4. CONCLUSIONS

The addition of K increases the density and strength of basic sites and the areal rates of aldol condensation chain growth reactions. Ethanol dehydrogenation is a structure-insensitive reaction that requires exposed Cu sites for its rate-determining elementary steps. Cu sites also play a critical role in condensation reactions. Alcohol chain growth reactions occur via bifunctional (metal-base) pathways requiring both Cu and basic sites. C–H bond activation steps on acid–base site pairs on basic oxides are coupled kinetically with recombinative desorption on Cu sites during reactions of alcohols on K–$Cu_yMg_5CeO_x$ catalysts.

Isotopic tracer studies using $^{12}C_2H_5OH$–$^{13}C_2H_4O$ reactant mixtures confirm that condensation reactions can proceed via direct reactions of ethanol without the intermediate formation of gas phase acetaldehyde molecules. The effect of Cu surface area on the rate of deuterium incorporation into the unreacted ethanol is consistent with the proposed bifunctional mechanism, in which Cu sites increase the rate of aldol condensation by removing surface hydrogen that tends to reverse the step forming the unsaturated aldol-type species required for chain growth. Isotopic tracer studies of alcohol coupling reactions suggest that chain growth occurs by the addition of a methanol-derived C_1 species to adsorbed oxygenates. These studies also show that aldol condensation reactions of alcohols are reversible on metal-base bifunctional catalysts at these reaction conditions.

ACKNOWLEDGMENTS

This work was supported by Division of Fossil Energy of the United States Department of Energy under Contract DE-AC22-94PC94066. The authors thank Dr. M. Xu and Mr. Zhengjie Hu for their technical assistance with the CO_2 isotopic switch experiments and Drs. M. Xu and A. M. Hilmen for frequent discussion and helpful suggestions. M. J. L. Gines acknowledges the Universidad Nacional del Litoral, Santa Fe, Argentina for a postdoctoral fellowship.

REFERENCES

1. Keim, W., and Falter, W., *Catal. Lett.* **3**, 59 (1989).
2. Keim, W., D.E. Patent 3810421 (1988).
3. Lietti, L., Forzatti, P., Tronconi, E., and Pasquon, I., *J. Catal.* **126**, 401 (1990).
4. Forzatti, P., Tronconi, E., and Pasquon, I., *Catal. Rev. Sci. Eng.* **33**, 109 (1991).
5. Sofianos, A., *Catal. Today* **15**, 119 (1990).
6. Nunan, J. G., Bogdan, C. E., Klier, K., Smith K. J., Young, C.-W., and Herman R. G., *J. Catal.* **113**, 410 (1988).
7. Nunan, J. G., Bogdan, C. E., Herman, R. G., and Klier, K., *Catal. Lett.* **2**, 49 (1989).
8. Nunan, J. G., Bodgan, C. E., Klier, K., Smith, K., Young, C., and Herman, R. G., *J. Catal.* **116**, 195 (1989).
9. Nunan, J. G., Herman, R. G., and Klier, K., *J. Catal.* **116**, 222 (1989).
10. Slaa, J. C., van Ommen, J. G., and Ross, J. R. H., *Catal. Today* **15**, 129 (1992).
11. Apesteguia, C. R., Soled, S. L., and Miseo, S., U.S. Patent 5,387,570 (1995), assigned to Exxon Research and Engineering Co.
12. Apesteguia, C. R., DeRites, B., Miseo, S., and Soled, S. L., *Catal. Lett.* **44**, 1 (1997).
13. Xu, M., Gines, M. J. L., Hilmen, A. M., Stephens, B. L., and Iglesia, E., *J. Catal.* **171**, 130 (1997).
14. Chinchen, G. C., Denny, P. J., Jennings, J. R., Spencer, M. S., and Waugh, K. C., *Appl. Catal.* **36**, 1 (1988).
15. Waugh, K. C., *Catal. Today* **15**, 51 (1992).
16. Tsuji, H., Yagi, F., Hattori, H., and Kita, H., *J. Catal.* **148**, 759 (1994).
17. Radlowski, C. A., and Hagen, G. P., U.S. Patent 5,159,125, assigned to Amoco Corporation, Chicago, IL.
18. Ueda, W., Kuwabara, T., Ohshida, T., and Morizawa, Y., *J. Chem. Soc., Chem. Comm.* 1558 (1990).
19. Ueda, W., Kuwabara, T., Ohshida, T., and Morizawa, Y., *Catal. Lett.* **12**, 97 (1992).
20. Chinchen, G., Mansfied, K., and Spencer, M., *CHEMTECH* (1990).
21. Nakamura, J., Uchijima, T., Kanai, Y., and Fujitani, T., *Catal. Today* **28**, 223 (1996).
22. Bowker, M., Hadden, R. A., Houghton, H., Hyland, J. N. K., and Waugh, K. C., *J. Catal.* **109**, 263 (1988).
23. Chauvin, C., Saussey, J., Lavalley, J. C., Idriss, H., Hindermann, J. P., Kiennemann, A., Chaumette, P., and Courty, P., *J. Catal.* **121**, 56 (1990).
24. Robbins, J. L., Iglesia, E., Kelkar, C. P., and DeRites, B., *Catal. Lett.* **10**, 1 (1991).
25. Neophytides, S. G., Marchi, A. J., and Froment, G. F., *Appl. Catal. A* **86**, 45 (1992).
26. Joo, O. S., Jung, K. D., Han, S. H., Uhm, S. J., Lee, D. K., and Ihm, S. K., *Appl. Catal. A* **135**, 273 (1996).
27. Mazanec, T. J., *J. Catal.* **98**, 115 (1986).
28. Fox, J. R., Pesa, F. A., and Curatolo, B. S., *J. Catal.* **90**, 127 (1984).
29. Elliot, D. J., and Pennella, F., *J. Catal.* **114**, 90 (1988).
30. Vedage, G. A., Himelfarb, P. B., Simmons, G. W., and Klier, K., *ACS Symp. Ser.* **279**, 295 (1985).
31. Xu, M., and Iglesia, E., *Catal. Lett.*, in press.
32. Xu, M., and Iglesia, E., unpublished results.
33. Loudon, G. M., "Organic Chemistry," 2nd ed., Benjamin/Cummings, Redwood City, CA, 1988.
34. Elliot, D. J., and Pennella, F., *J. Catal.* **119**, 359 (1989).
35. Chinchen, G. C., Hay, C. M., Vandervell, H. D., and Waugh, K. C., *J. Catal.* **103**, 79 (1987).
36. Iglesia, E., and Boudart, M., *J. Catal.* **81**, 204 (1983).
37. Scholten, J. J., and Kovanlinka, J. A., *Trans. Faraday Soc.* **65**, 2454 (1969).
38. Xu, M., and Iglesia, E., *J. Phys. Chem.* **102**, 961 (1998).
39. Price, G. L., and Iglesia, E., *Ind. Eng. Chem.* **28**, 839 (1989).
40. McKenzie, A. L., Fishel, C. T., and Davis, R. J., *J. Catal.* **138**, 547 (1992).
41. Lamonier, C., Bennani, A., Duysser, A., and Wrobel, G., *J. Chem. Soc., Faraday Trans.* **92**(1), 131 (1996).
42. Soria, J., *Solid State Ionics* **63–65**, 755 (1993).
43. Takezawa, N., Hanamaki, C., and Kobayashi, H., *J. Catal.* **38**, 101 (1975).
44. Parrott, S. L., Roger, W., and White, J. M., *Applications of Surf. Sci.* **1**, 443 (1978).
45. Mole, T., Anderson, J. R., and Creer, G., *Appl. Catal.* **17**, 141 (1985).
46. Biscardi, J. A., and Iglesia, E., *Catal. Today* **31**, 207 (1996).
47. Iglesia, E., Barton, D. G., Biscardi, J. A., Gines, M. J. L., and Soled, S. L., *Catal. Today* **38**, 339 (1997).
48. Norman, R., and Coxon, J. M., *Principles of Organic Synthesis,* 3rd ed., Blackie Academic, Glasgow/London, 1993.
49. Chung, M. J., Moon, D. J., Kim, H. S., Park, K. Y., and Ihm, S. K., *J. Molec. Catal. A: Chemical* **113**, 507 (1996).
50. Hilmen, A.-M., Xu, M., Gines, M. J. L., and Iglesia, E., *Appl. Catal.*, in press.